Nanostructuring Platinum Nanoparticles on Multilayered Graphene Petal Nanosheets for Electrochemical Biosensing

*Jonathan C. Claussen, Anurag Kumar, David B. Jaroch, M. Haseeb Khawaja, Allison B. Hibbard, D. Marshall Porterfield, and Timothy S. Fisher**

Hybridization of nanoscale metals and carbon nanotubes into composite nanomaterials has produced some of the best-performing sensors to date. The challenge remains to develop scalable nanofabrication methods that are amenable to the development of sensors with broad sensing ranges. A scalable nanostructured biosensor based on multilayered graphene petal nanosheets (MGPNs), Pt nanoparticles, and a biorecognition element (glucose oxidase) is presented. The combination of zero-dimensional nanoparticles on a two-dimensional support that is arrayed in the third dimension creates a sensor platform with exceptional characteristics. The versatility of the biosensor platform is demonstrated by altering biosensor performance (i.e., sensitivity, detection limit, and linear sensing range) through changing the size, density, and morphology of electrodeposited Pt nanoparticles on the MGPNs. This work enables a robust sensor design that demonstrates exceptional performance with enhanced glucose sensitivity (0.3 μM detection limit, 0.01–50 mM linear sensing range), a long stable shelf-life (>1 month), and a high selectivity over electroactive, interfering species commonly found in human serum samples.

1. Introduction

Nanostructures have recently been utilized in a variety of biosensing applications due to their enhanced surface area, precise biomolecule-electrode connections, and enhanced delivery of amplication agents.[1–5] For electrochemical sensing, conductive nanostructures immobilized on electrodes enhance electrocatalytic behavior due to quantum confinement and exhibit unique properties including more favorable Faradic-to-capacitive current ratios, higher current densities, and faster mass transport by convergent diffusion than their larger micro/macro electrode counterparts.[6,7] In order to increase biosensor current output to measurable levels, large arrays of nanostructures (*i.e.*, nanoelectrode arrays [NEAs]), have been immobilized on electrode surfaces.[8,9] These NEA biosensors, fabricated with various nanostructures (*e.g.*, nanowires, nanotubes, and nanocrystals) have shown promising results, displaying high sensitivities and fast response times; however, the concomitance of a scalable fabrication technique, robust biofunctionalization scheme, and enhanced performance (*i.e.*, low detection limit and wide linear sensing range) remains to be seen.

To bridge the gap between fundamental research and commercial biosensor applications, fundamental nanoelectrode array fabrication challenges still need to be addressed including protocols for efficient electrode development and enzyme immobilization. Existing nanoelectrode fabrication protocols typically require lithography and chemical processing steps that are expensive, limited to serial processing, and not suitable for a wide variety of materials.[10] Templated development of nanoelectrode arrays with anodic alumina or polycarbonate generally eliminates the need for lithography, but still requires multi-step fabrication protocols (*e.g.*, physical vapor deposition, anodization, and electrodeposition) to develop the template and subsequent nanostructures.[11,12] Similarly, biosensors comprised of ordered and semi-ordered arrays of carbon nanotubes (CNTs) typically require template development or lithography to geometrically distribute metal catalysts and/or chemical functionalization steps to prepare CNTs for conjugation with biorecognition agents.[13–15] However, recently developed graphene petal nanosheets with highly reactive edge planes can be grown directly on a variety of surfaces without the need for metal catalysts—creating a nanostructured surface well suited for integration into numerous electrochemical sensing applications.[16–18]

Various biofunctionalization techniques have been developed to immobilize biorecognition agents onto electrode surfaces including covalent binding through self-assembled monolayers (SAMs), non-covalent membranes, and electrodeposition with conductive polymers. Self-assembled monolayers provide

A. Kumar, M. H. Khawaja, A. B. Hibbard, Prof. T. S. Fisher
Birck Nanotechnology Center
Department of Mechanical Engineering
Purdue University
1205 W. State St., West Lafayette, IN 47907-2057 USA
E-mail: tsfisher@purdue.edu
Dr. J. C. Claussen, Prof. D. M. Porterfield
Birck Nanotechnology Center
Department of Agricultural and Biological Engineering
Purdue University, USA
D. B. Jaroch, Prof. D. M. Porterfield
Birck Nanotechnology Center
Weldon School of Biomedical Engineering
Purdue University, USA

DOI: 10.1002/adfm.201200551

a strong and stable covalent link to the biorecognition agent and electrode surface; but they also create an electron-transfer barrier that can impede heterogeneous charge transport and diminish biosensor sensitivity.[12,19,20] Non-covalent membranes can be rapidly assembled on electrode surfaces, but they are subject to delamination and show limited reproducibility in biological sensing applications.[21] However poly(3,4-ethylenedioxythiophene) (PEDOT) is an electrically conductive polymeric material that can be utilized in biosensor interfaces due to its biocompatibility, stability, and high conductivity.[22,23] Mixtures of the monomer 3,4-ethylenedioxythiophene (EDOT) and Poly(styrene-sulfonate) (PSS) are soluble in aqueous environments and can be controllably electrodeposited onto conductive surfaces.[24] Furthermore PEDOT displays high stability with aqueous electrolytes.[23] This high electrochemical stability, owing to inherent dioxyethylene bridging groups, makes PEDOT well suited for enzyme immobilization matrixes as reported for use in glucose[25] and cholesterol[26] amperometric biosensing applications.

In this paper we present a fundamentally new nanostructured biosensor to address many of the limitations that nanoelectrode array biosensors currently face. In lieu of lithography/etch back fabrication techniques, porous templates, or metal catalyst driven carbon nanotube arrays we grow multilayered graphene petal nanosheets (MGPNs) on a silicon wafer through a chemical vapor deposition technique. The MGPNs act as a highly conductive template for subsequent Pt nanoparticle electrodeposition—nanoparticles that are well know for their cataltyic behavior in fuel cells,[27,28] hydrogen storage,[29] chemical sensors,[30] and biosensors.[31–33] A one-step electrodeposition process is used to grow platinum nanoparticles (PtNPs) along the graphene petal edges and planes to enhance electrochemical performance. The size and density of the PtNPs are manipulated to maximize the biosensor sensitivity and dynamic sensing range. A robust sensor biofunctionalization protocol is used to electrodeposit enzyme with the electrically conductive polymer Poly(3,4-ethylenedioxythiophene) (PEDOT) onto the electrode surface. In order to benchmark the performance against the broadest collection of biosensors, the enzyme glucose oxidase (GOx) (perhaps the most widely studied enzymatic biosensing paradigm since its inception from Clark and Lyons in 1962),[34,35] is encapsulated within the PEDOT matrix for subsequent amperometric glucose sensing. The optimized PtNP-MGPN glucose biosensor performance proves to be exemplary with strong glucose sensitivity even after 5 weeks of use, minimal interference from endogenous electroactive species (*i.e.*, ascorbic acid, uric acid, and acetaminophen) typically found in human serum samples, and a low detection limit and wide linear sensing range that greatly improves upon the performance of glucose biosensors previously reported in the literature.

2. Results

2.1. Multilayered Graphene Petal Nanosheet (MGPN) Electrodes

An array of MGPNs were grown across a Ti-coated silicon substrate using a microwave plasma chemical vapor deposition technique (see Experimental Methods). The petals uniformly grow across the surface of the electrode —protruding a distance of approximately 500 nm from the surface (**Figure 1**). The 1–10 nm thickness of the petals (measured by a Veeco atomic force microscope) and the average 12 layer graphene depth measured by tunneling electron microscopy (Figure S1 in Supporting Information) are consistent with previous reported morphologies corresponding to 5–25 graphene layers.[16,17] In an effort to increase the electroactive nature of the MGPN electrodes and improve subsequent PtNP deposition, the MGPN electrodes were exposed uniformly to a 30 second oxygen plasma etch. The effects of this etching process were characterized with Raman spectroscopy, ferricyanide cyclic voltammetry, and amperometric hydrogen peroxide (H_2O_2) sensing (Figure S2 in Supporting Information). These spectroscopy and electrochemical characterization experiments corroborate previous studies that demonstrate plasma etching improves electrochemical performance and subsequent metallic nanoparticle deposition on HOPG,[36] carbon nanowalls,[17] and carbon nanotubes.[37] Such improvements can be attributed to the O_2 plasma etch generating defects and oxygenated species on the superficial graphene layers. The generated defects render the graphene surface more electroactive than the untreated, superficial basal planes,[38,39] while newly formed oxygenated species alter the electrode nature from hydrophobic to hydrophilic—enhancing the ability of electrolyte to impregnate the carbon surface.[40]

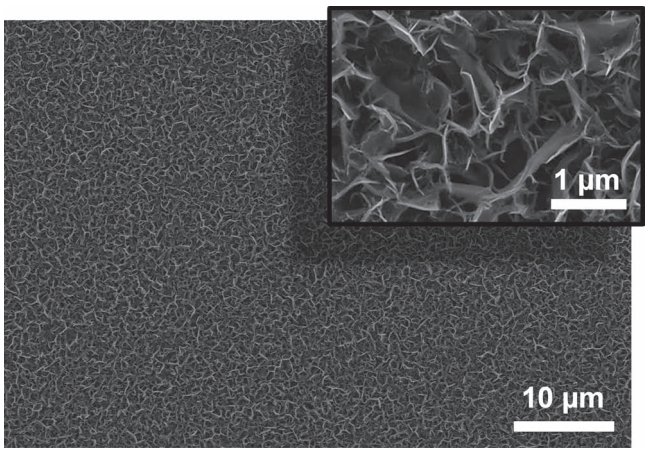

Figure 1. Field emission scanning electron microscopy (FESEM) microscopy images of a MGPN electrode grown by microwave plasma chemical vapor deposition (MPCVD) on a Ti coated silicon substrate. Inset shows a magnified view.

2.2. Platinum Nanoparticle (PtNP) Modified MGPN Electrodes

In an effort to increase electro-reactivity towards H_2O_2 oxidation,[13,33,41] Pt nanoparticles of varying size, density, and morphology are electrodeposited onto the MGPNs (**Figure 2**). Pt nanoparticles are electrodeposited through a current pulse technique with a similar 3-electrode set-up as mentioned previously (see Experimental Section). Five distinct currents are used to create five Pt-MGPN electrodes with Pt nanoparticles of unique

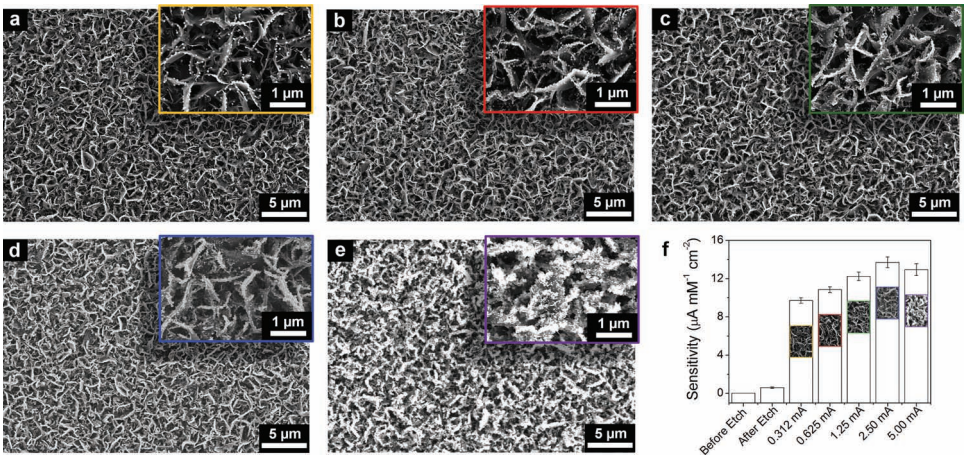

Figure 2. Characterization of the platinum nanoparticle modified multilayered graphene petal nanosheet (PtNP-MGPN) electrodes before enzyme immobilization. (a-e) Field emission scanning electron microscopy (FESEM) micrographs of PtNPs electrodeposited on MGPNs. Current pulses (500 ms) of (a) 312 μA (orange), (b) 625 μA (red), (c) 1.25 mA (green), (d) 2.5 mA (blue), and (e) 5.0 mA (purple) were used to electrodeposit Pt nanoparticles of distinct size and density onto the MGPNs. (f) Bar graph displaying the H_2O_2 sensitivity of the MGPN electrode (before and after the oxygen plasma etch) and the PtNP-MGPN electrodes. Errors bars show standard deviation for 3 different experiments.

size, density, and morphology. Current pulses of 312 μA initiate nanoparticle growth along the MGPN ridge lines with an average nanoparticle width of (46 ± 5) nm and a nearly smooth to cauliflower-like morphology. The ridgeline nanoparticles grow to (86 ± 5) nm at 625 μA current pulses while nanoparticles (<20 nm, cauliflower-like morphology) began to form on each petal face. Ridgeline nanoparticles begin to coalesce at current pulses of 1.25 mA with average widths of (100 ± 10) nm with needle-like morphology while petal face nanoparticles (<20 nm) with cauliflower-like morphology become more apparent. At 2.5 mA the petal tips are almost entirely coated with needle-like Pt nanoparticles (<10 nm in width) extending from the ridgeline nanoparticles (width of (100 ± 25) nm) while all visible petal faces contain an array of needle-like Pt nanoparticles (<10 nm in width) extentding from petal face nanoparticles (<20 nm). At 5.0 mA the Pt ridgelines have now expanded in width to (300 ± 50) nm with a rose-like morphology while the petal face nanoparticles have grown to (35 ± 10) nm with a needle-like to rose-like morphology. Thus by changing the pulse deposition current the Pt nanoparticle size, density, and morphology can be altered.[31,42] These distinct Pt nanoparticle characteristics have a significant and unique impact on subsequent H_2O_2 and glucose sensing.

Amperometric H_2O_2 calibration plots were performed in the same manner as mentioned previously with a working potential of 500 mV. The H_2O_2 sensitivity of the MGPN electrode is greatly enhanced with the introduction of Pt as the sensitivity increases from 0.595 mA mM^{-1} cm^{-2} (MGPN electrode after oxygen plasma etch) to 9.71 mA mM^{-1} cm^{-2}, an increase of more than 16 fold, after Pt electrodeposition with 312 μA current pulses. The H_2O_2 sensitivity increases as a function of the Pt electrodeposition current pulse until a maximum sensitivity of 13.7 mA mM^{-1} cm^{-2} is reached for the Pt-MGPN biosensor with 2.50 mA current pulses. The H_2O_2 sensitivity decreases to 12.9 mA mM^{-1} cm^{-2} for the Pt-MGPN biosensor with 5.0 mA current pulses. As a supplementary control experiment, Pt was electrodeposited onto planar highly ordered pyrolytic graphite (HOPG) at the same conditions (2.5 mA current pulses, 250 cycles) as the optimized Pt-MGPN electrode. The H_2O_2 sensitivity of the optimized Pt-MGPN was nearly 5 times as great as the Pt-HOPG electrode—illustrating the enhanced sensitivity of MGPNs over conventional carbon-based substrates (Figure S3 in Supporting Information).

2.3. Glucose Sensing

In order to convert the PtNP-MGPN electrodes into enzymatic biosensors, the enzyme GOx is mixed with the conductive polymer PEDOT and subsequently electrodeposited onto the electrode surface (see Experimental Section). The PEDOT grain size can alter the conductivity of the deposited PEDOT film.[43] Since the GOx-PEDOT layer was electrodeposited under the same conditions for all 5 Pt-MGPN samples [constant current pulses of 1.05 mA that are applied between the working electrode (Pt-MGPN) and auxiliary electrode (Pt gauze) for 500 cycles] aberrations in grain size and average thickness between electrode samples are considered to be negligible. Thus the conductivity of the PEDOT and amount of GOx enzyme electrodeposited on each MGPN electrode is considered equivalent.

During electrochemical glucose sensing, where glucose is the substrate of GOx, generated hydrogen peroxide (H_2O_2) is subsequently oxidized at the electrode surface, producing a measurable current signal (Equation 1 & 2). A schematic portraying the biofunctionalized PtNP-MGPN glucose biosensors as well as the enzymatic function of GOx is illustrated in **Figure 3**a.

$$\text{D}-\text{glucose} + \text{O}_2 + \text{H}_2\text{O} \xrightarrow{\text{GOx}} \text{D}-\text{gluconic acid} + \text{H}_2\text{O}_2 \quad (1)$$

$$\text{H}_2\text{O}_2 \rightarrow 2\text{H}^+ + \text{O}_2 + 2\text{e}^- \quad (2)$$

Amperometric glucose sensing is carried out in the same 3-electrode set-up and working potential (500 mV) as the amperometric H_2O_2 testing. Amperometric glucose calibration plots for all 5 PtNP-MGPN biosensors are created by adding successive aliquots of increasing concentrations of glucose and measuring the corresponding steady-state signal response, typically achieved within 5 seconds (Figure 3). The glucose sensitivity for the Pt-MGPN biosensors and linear sensing range of the PtNP-MGPN glucose biosensors follow similar trends found in the amperometric H_2O_2 testing where values continue to increase for higher Pt electrodeposition current pulses until a maximum sensitivity and linear sensing range is reached for the PtNP-MGPN biosensor with 2.50 mA current pulses (**Figure 4**). The

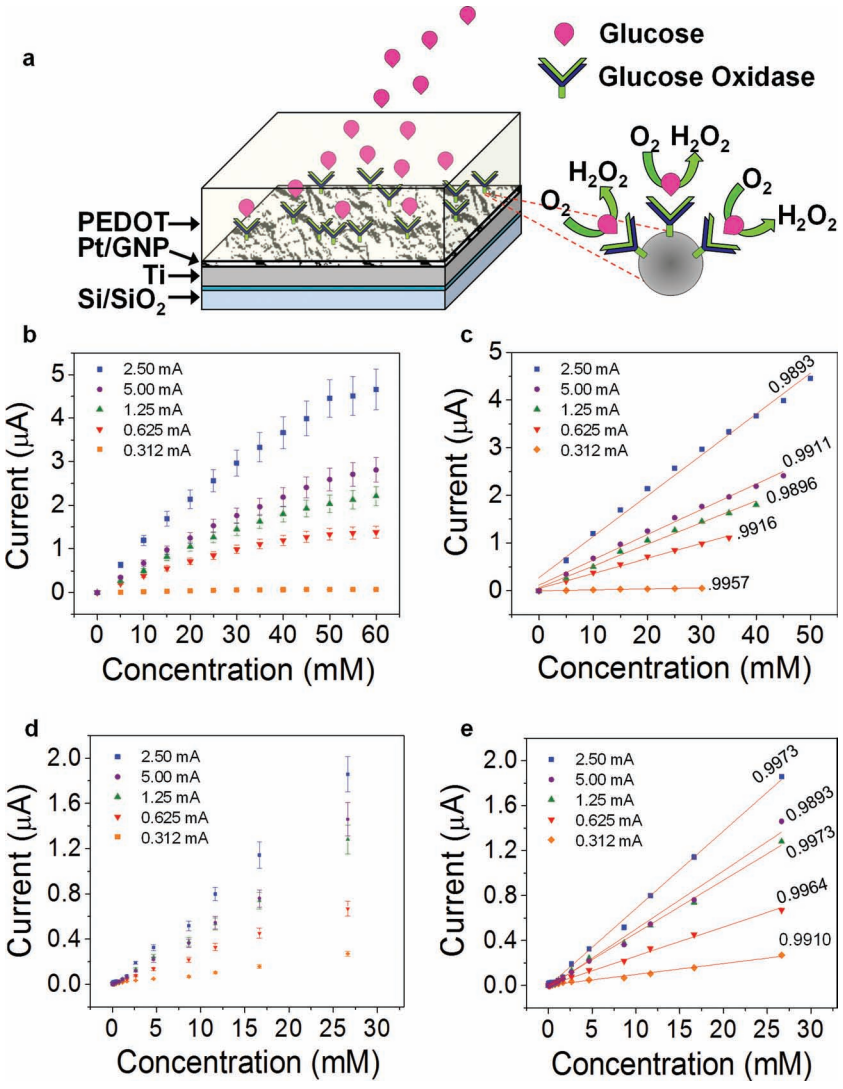

Figure 3. (a) Tilted cross-sectional schematic illustrating the GOx/PEDOT biofunctionalized PtNP-MGPN glucose biosensor with adjacent magnified view portrayal of GOx immobilized on a single PtNP. Glucose binds within the GOx enzymatic pocket producing H_2O_2 while consuming O_2. (b) Glucose calibration plots of the Pt-MGPN biosensors [Pt electrodeposition current pulses of 312 μA (orange), 625 μA (red), 1.25 mA (green), 2.5 mA (blue), and 5.0 mA (purple)] portrays the dynamic current response for a glucose concentration range of 5–60 mM by 5 mM aliquots and (c) corresponding linear glucose sensing range with linear regression analysis and coefficient of determination (R^2) as illustrated. (d) Glucose calibration plot for a glucose concentration range of 0.01 mM to 26.65 mM by incremental glucose concentration steps of 10–50 μM by 10 μM, 100-500 μM by 100 μM, 1–5 mM by 1 mM, followed by one step of 10 mM glucose and (e) corresponding linear glucose sensing range and coefficient of determination (R^2) as illustrated.

glucose detection limit (S/N = 3, signal-to-noise ratio of 3) and linear sensing range of the optimized Pt-MGPN biosensor is listed and compared to glucose biosensors comprised of similar materials including graphene, carbon nanotubes, and PtNPs (**Table 1**).

To our knowledge, the sensing range of the optimized Pt-MGPN biosensor is wider respectively than any other nanostructured biosensors reported in the literature. Furthermore, the broad linear sensing range of the Pt-GPN biosensor not only enables sensing within the physiological range for blood glucose of healthy [3.6 mM and 7.5 mM (65 mg/dL–135 mg/dL)] and diabetic [1.1 mM and 20.8 mM (20 mg/dL–350 mg/dL)] patients;[54] it enables glucose sensing in saliva,[55] tears,[56] and urine[57] as well. Thus this wide linear sensing range opens possibilities for new non-invasive sensing protocols in which glucose levels from diverse human serums could be monitored simultaneously (Figure 4a).

2.4. Biosensor Lifetime Performance and Selectivity

The durability of the GOx/PEDOT electrodeposition technique has been validated by performing glucose biosensing measurements over a 5-week period. Between weekly testing, the sensors remain within a capped petri dish with no refrigeration—mimicking off-the-shelf storage typical of home blood glucose monitoring systems. The optimized Pt-MGPN biosensor retains more than 75% of its sensitivity even after 5 weeks of testing—demonstrating the robust nature of the enzyme immobilization protocol with cyclic testing and storage (Figure 4b). The glucose selectivity of the optimized PtNP-MGPN glucose biosensor (Pt electrodeposition of 5 mA) has also been tested by sensing glucose within three known electroactive species (uric acid (UA), acetaminophen (AP), and ascorbic acid (AA)), commonly found in human serum samples. A glucose concentration of 5 mM electrochemically monitored after the addition of 100 μM aliquots of AP, UA, and AA exhibits minimal interference from endogenous electroactive species (Figure 4c).

3. Conclusions

We have shown the first example of using multilayered graphene petal nanosheets (MGPNs) in an electrochemical biosensing application. Few prior reports of sensing with MGPNs are available, but initial research has begun to uncover favorable electrochemical properties stemming from the exposed petal tips that exhibit the fast ET rates typically found in graphene edge planes.[18] In this work, we introduce the concept of using the MGPNs as templates for Pt nanoparticle growth to enhance the electro-reactivity of the petals and, in effect, present a nanoelectrode array fabrication protocol that eliminates the complexity of traditional NEA designs that typically includes anodic alumina or polycarbonate templates and/or multi-step lithography steps. These Pt nanoparticle/MGPNs outperform conventional planar Pt nanoparticle/

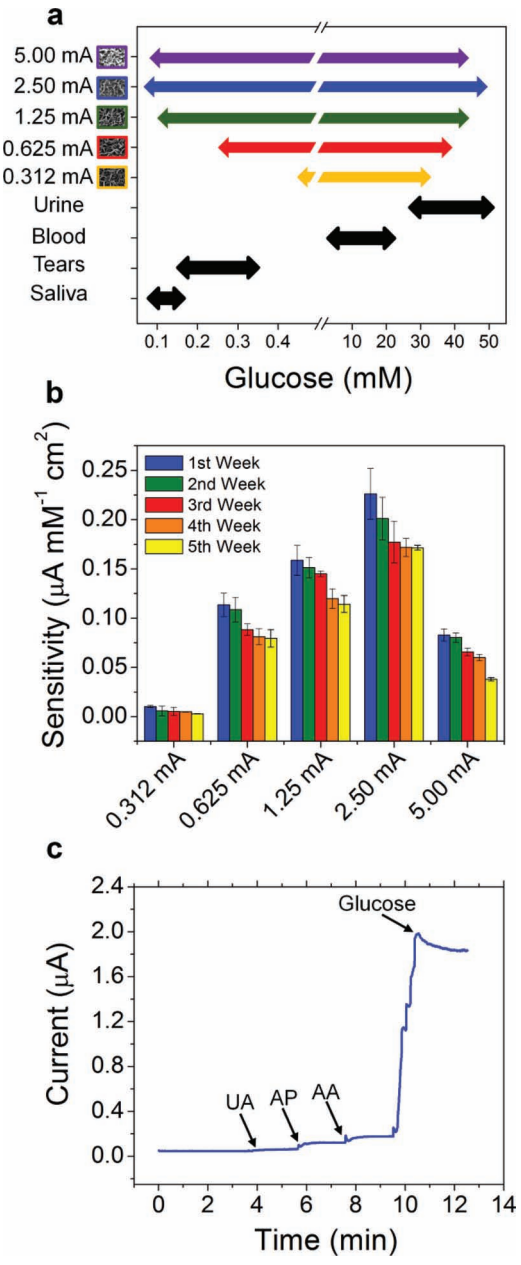

Figure 4. (a) Glucose sensing ranges of the Pt-MGPN glucose biosensors [Pt electrodeposition current pulses of 312 μA (orange), 625 μA (red), 1.25 mA (green), 2.5 mA (blue), and 5.0 mA (purple)] as compared to glucose levels found in urine, blood, tears, and saliva. (b) Biosensor lifetime measurements where the glucose sensitivity for each distinct Pt-MGPN glucose biosensor was monitored over a period of 5 weeks. (c) Selectivity test demonstrating minimal interference from 100 μM aliquots of uric acid (UA), acetaminophen (AP), and ascorbic acid (AA) and successful detection of glucose (5 mM) within the backdrop of said electroactive, interfering species for the Pt-MGPN glucose biosensor (Pt electrodeposition of 2.5 mA).

HOPG in terms of H_2O_2 sensitivity (~5:1 respectively), thus demonstrating the impact nanostructured, three dimensionally arrayed MGPNs fused with Pt nanoparticles can exhibit in electrochemical sensing.

Table 1. Electrochemical biosensor performance comparison of glucose biosensors based upon, graphene/graphite, carbon nanotubes, and metallic nanoparticles.

Biosensor	Base Material	Detection Limit [μM]	Sensing Range [mM]	Ref.
GOx-PEDOT/PtNP/MGPNs	Graphene/Graphite	0.3	0.01–50	this work
GOx-Nafion-Pt-xGnPs	Graphene/Graphite	1	1–20	[44]
Ppy-GOx-Gn	Graphene/Graphite	3	.002–.040	[45]
GOx-CNx-MWCNTs	Carbon Nanotubes	10	.02–1.02	[46]
GOx-Fc-MWCNTs	Carbon Nanotubes	3	.012–3.8	[47]
GOx-HRP-Ppy-SWCNT	Carbon Nanotubes	30	.03–2.43	[48]
GOx-Nafion/AuNPs-MWCNTs	Carbon Nanotubes	20	0.05–22	[49]
GOx-PtNPs-SWCNTs	Carbon Nanotubes	0.5	0.005–5	[41]
GOx-PtNPs-CNTs/TiO_2	Carbon Nanotubes	5.7	0.006–1.5	[50]
GOx/aligned-SWCNTs	Carbon Nanotubes	80	up to 30	[15]
GOx/AuNWs-CS	Metallic Nanoparticles	5	.01–10	[51]
GOx-CS-IL/AuNPs	Metallic Nanoparticles	1.5	0.003–9	[52]
GOx-CS-Nafion/AuNPs	Metallic Nanoparticles	2.7	.005–2.4	[53]

(GOx)–glucose oxidase, (xGnPs)–exfoliated graphite nanoplatelets, (Gn)–graphene, (Ppy)–polypyrrole, (MWCNT)–multi-walled carbon nanotubes, (SWCNT)–single-walled carbon nanotube, (PtNPs)–platinum nanoparticles, (AuNPs)–gold nanoparticles, (AuNWs)–Au nanowires, (CNx-MWCNTs)–nitrogen doped multi-walled carbon nanotubes, (Fc)–ferrocenecarboxaldehyde, (HRP)–horseradish peroxidase, (CS)–chitosan, (IL)–ionic liquid

The link between electrode nanostructuring and enzymatic biosensing sensitivity remains relatively unexplored in the literature. Soleymani and co-workers have begun to piece together the relationship between biodetection sensitivity and controlled nanostructuring through their work with palladium microelectrodes and nucleic acid detection.[3,58] The work presented in this manuscript further elucidates the subject, by demonstrating how Pt nanoparticle size, morphology, and density can be controlled to improve the linear sensing range and the detection limit of the enzymatic biosensors. MGPN electrodes decorated with densely-packed (*i.e.*, particles covering the graphene petal ridgelines and peppering the graphene petal faces), needle-like Pt nanoparticles yieled the best results in terms of hydrogen peroxide and glucose sensing—corroborating similar reports connecting tightly-packed densities and needle-like morphologies of Pt nanoparticles immbolized on carbon substrates to higher electroreactive ability.[31,42,59] This optimization process

yields outstanding results in the glucose sensing paradigm by widening the glucose sensing range into the physiological concentration levels found in urine, tears, and saliva in addition to blood.

The electrodeposition of GOx with PEDOT onto the PtNP modified MGPNs enables robust glucose sensing with minimal interference for over one month from endogenous electroactive species commonly found in human serum samples. The results of the selectivity experiments can be explained in part by the electrodeposited PEDOT layer. The electrodeposition of PEDOT at high concentrations (> = 1 mA) as performed in this work can over-oxidize carbon atoms on the polymer backbone—transforming the PEDOT polymer chain charge from positive to partially negative.[60,61] Thus the electrodeposited PEDOT tends to repel negatively-charged electrochemical interferents (*e.g.*, ascorbic and uric acid) due to electrostatic repulsion during electrochemical biosensing.

The bottom-up growth of MGPNs on a silicon wafer, electrodeposition of Pt nanoparticles, and electrodeposition of enzyme encapsulated within the conductive polymer PEDOT are all scalable fabrication techniques that can be potentially integrated into a wide array of electronic devices. This work should have a tremendous impact on biosensing, and in a broader context the field of electrochemical sensing as fabrication protocols presented herein facilitate rapid sensor development, sensitivity tuning techniques, and biorecognition longevity that is not accessible in many sensor design protocols. This high-sensitivity biosensing platform can be quite versatile as the GOx can be interchanged with other enzymes such as glutamate oxidase, lactate oxidase, and alcohol oxidase for the advancement of basic research and in-field sensing of biomarkers associated with neurological disorders,[60] patient trauma,[62,63] food quality,[64] and next generation bio-ethanol fuel technologies.[65] Furthermore, these fabrication protocols are amenable to lab-on-a-chip platforms where the MGPNs, PtNPs, and respective enzymes can all be electrodeposited onto distinct microelectrodes for multi-plexed biosensing purposes. Thus we believe the PtNP-MGPN biosensor technology will not only improve fundamental physiology research, it will enable multiplexed monitoring of numerous analytes associated with medicine, agriculture, food safety, and security.

4. Experimental Section

Base electrode fabrication: A thin film of Ti (100 nm) is e-beam evaporated onto an oxidized silicon wafer [P <100> Si (5 μm), SiO_2 (500 nm)] at a base pressure of 5.0 × 10-7 Torr. The metalized wafer is diced with a diamond-blade dicing saw (Disco DAD-2H/6) into equally-sized electrodes (0.35 cm^2) after a thin film of AZ1518 photoresist is spun and hardbaked (10 min at 120 °C) unto the wafer to protect the surface during cutting operation. After wafer dicing, the electrodes are solvent cleaned with acetone, methanol, and isopropyl alcohol and subsequently dried under a gentle stream of N_2 gas to remove the photoresist and debris before MGPN Synthesis.

Multilayered graphene petal nanosheet (MGPN) synthesis: The growth of the MGPNs is carried out by microwave plasma chemical vapor deposition (MPCVD) with a SEKI AX5200S MPCVD reactor following similar protocols established in our previous work.[16,17] The Ti coated silicon electrodes are elevated 17 mm above a 5.1 cm diameter molybdenum puck, placed inside the MPCVD reactor chamber and heated to 700 °C in a hydrogen ambient by a 3.5 kW radio-frequency power supply at a pressure of 30 Torr. A hydrogen plasma is generated over the sample via a 5 kW SEKI AX5200S microwave generator, while methane (CH_4) gas, the acting precursor for MGPN growth, is pumped into the chamber for 10 minutes at a flow rate of 10 SCCM. The hydrogen plasma decomposes the methane gas to permit monolithic MGPN growth across the entire surface of the electrode (Figure 1).

Oxygen plasma etch: In an effort to improve the electroactive nature of the MGPNs, the MGPN electrode was exposed to an O_2 plasma etch within a Plasma Tech Reactive Ion Etch (RIE). The MGPN electrode was placed inside the vacuum chamber of the reactor and pumped down to a base pressure of 0.1 mTorr to eliminate/minimize contaminating species that may have been introduced into the chamber during loading. O_2 was introduced into the chamber at a flow rate of 50 SCCM and the chamber pressure was adjusted to 60 mTorr. A O_2 plasma was generated over the MGPN electrode for 30 seconds by setting the RF generator to the 100 W power setting.

Pt nanoparticle electrodeposition: A 3 electrode electrochemical set-up (BASi Epsilon Three-Electrode Cell Stand - potentiostat) where the MGPNs acted as the working electrode, Pt gauze as the auxiliary electrode, and Ag/AgCl as the reference electrode were dipped within a plating solution consisting of $H_2PtCl_6{\cdot}6H_2O$ (4 mM, Sigma Aldrich 206083) and Na_2SO_4 (0.5 M, Fluka 71960) to electrodeposit Pt nanoparticles onto the MGPN electrodes. Current pulses (500 ms) of 312 uA, 625 uA, 1.25 mA, 2.5 mA and 5.0 mA were utilized in cycles of 250 to manipulate the size, density, and morphology of Pt nanoparticles deposited on the MGPNs.

Glucose oxidase (GOx) immobilization: Glucose oxidase is mixed with Poly(3,4-ethylenedioxythiophene) (PEDOT) before it is electrodeposited onto the PtNP-MGPN electrodes. The GOx/PEDOT solution is created by first mixing poly(styrenesulfonate) (0.1 M) in H_2O. Next, 3,4-ethylenedioxythiophene (0.03 M, Sigma Aldrich 483028) is added to the mixture while the solution is agitated. The enzyme glucose oxidase (GOx) (Sigma Aldrich G7141) dissolved in H_2O (2 mg/ml) is next added to the mixture. The subsequent PEDOT/GOx solution is electrodeposited onto each Pt-MGPN electrode via constant current pulses of 1.05 mA that are applied between the working electrode (Pt-MGPN) and auxiliary electrode (Pt gauze) for 500 cycles.

Electrochemical measurements/set-up: All electrochemical testing was performed in a 3 electrode set-up (BASi Epsilon Three-Electrode Cell Stand - potentiostat) where the MGPN or PtNP-MGPN electrodes acted as the working electrode, a Pt wire as the auxiliary electrode, and Ag/AgCl as the reference electrode. Amperometric hydrogen peroxide (H_2O_2) and glucose sensing experiments were performed in phosphate buffered saline (PBS, 0.1 M pH 7.4) at a working potential of 500 mV under constant stirring (500 rpm) with a 0.5 cm (length) magnetic stir bar while successive increasing concentration aliquots of said target analyte were pipetted into the testing vial. The Pt-MGPN biosensors act as small electrochemical dipsticks were the sensor region (0.35 cm^2) of the electrode is masked by an acid resistant lacquer. The horizontal lacquer line (0.2 cm wide) separates the dipstick in half, where one end is submerged in the testing solution and the other end is electrically wired to the potentiostat via an alligator clip and cable connecting wire. In the testing vial, the nanostructured dipsticks are submerged to the midpoint of the lacquer line so small variations in fluid levels during testing do not change the submerged surface area. Since each dipstick is diced and lacquer coated in an identical manner, each dipstick has a submergible sensor region of 0.35 cm^2.

Raman Spectroscopy: Raman spectroscopy was performed using a T64000 system by Horiba Scientific. All the spectra were collected at room temperature using a laser excitation at 488 nm wavelength. The laser power was 2 mW and a 50X objective lens was used.

Sensor Imaging: A S-4800 Hitachi microscope was utilized at a power setting of 5.0 kV to obtain all field emission scanning electron microscopy (FESEM) micrographs. No additional processing steps were required before image analysis.

Supporting Information

Supporting Information is available from the Wiley Online Library or from the author.

Acknowledgements

The authors gratefully acknowledge assistance from the Purdue Physiological Sensing Facility and Purdue Nanoscale Transport Research Group of the Birck Nanotechnology Center and Bindley Bioscience Center. We recognize funding support from the Office of Naval Research, National Science Foundation, and the Purdue Research Foundation Trask Fund.

Received: February 25, 2012
Published online: May 9, 2012

[1] P. Alivisatos, *Nat. Biotechnol.* **2004**, *22*, 47.
[2] M. Dankerl, M. V. Hauf, A. Lippert, L. H. Hess, S. Birner, I. D. Sharp, A. Mahmood, P. Mallet, J.-Y. Veuillen, M. Stutzmann, J. A. Garrido, *Adv. Funct. Mater.* **2010**, *20*, 3117.
[3] L. Soleymani, Z. Fang, E. H. Sargent, S. O. Kelley, *Na. Nanotechnol.* **2009**, *4*, 844.
[4] Y. Xiao, F. Patolsky, E. Katz, J. F. Hainfeld, I. Willner, *Science* **2003**, *299*, 1877.
[5] Q. Zeng, J. Cheng, L. Tang, X. Liu, Y. Liu, J. Li, J. Jiang, *Adv. Funct. Mater.* **2010**, *20*, 3366.
[6] R. G. Compton, G. G. Wildgoose, N. V. Rees, I. Streeter, R. Baron, *Chem. Phys. Lett.* **2008**, *459*, 1.
[7] C. N. R. Rao, G. U. Kulkarni, P. J. Thomas, P. P. Edwards, *Chem. Eur. J.* **2002**, *8*, 28.
[8] Y. H. Lanyon, D. W. M. Arrigan, *Sens. Actuators, B* **2007**, *121*, 341.
[9] M. E. Sandison, J. M. Cooper, *Lab Chip* **2006**, *6*, 1020.
[10] M. S. Sander, L. S. Tan, *Adv. Funct. Mater.* **2003**, *13*, 393.
[11] D. Borissov, S. Isik-Uppenkamp, M. Rohwerder, *J. Phys. Chem. C* **2009**, *113*, 3133.
[12] J. C. Claussen, M. M. Wickner, T. S. Fisher, D. M. Porterfield, *ACS Appl. Mater. Interfaces* **2011**, *3*, 1765.
[13] J. C. Claussen, M. S. Artiles, E. S. McLamore, S. Mohanty, J. Shi, J. L. Rickus, T. S. Fisher, D. M. Porterfield, *J. Mater. Chem.* **2011**, *21*, 11224.
[14] J. C. Claussen, A. D. Franklin, A. ul Haque, D. M. Porterfield, T. S. Fisher, *ACS Nano* **2009**, *3*, 37.
[15] Y. Lin, F. Lu, Y. Tu, Z. Ren, *Nano Lett.* **2004**, *4*, 191.
[16] T. Bhuvana, A. Kumar, A. Sood, R. H. Gerzeski, J. Hu, V. S. Bhadram, C. Narayana, T. S. Fisher, *ACS Appl. Mater. Interfaces* **2010**, *2*, 644.
[17] C. S. Rout, A. Kumar, G. Xiong, J. Irudayaraj, T. S. Fisher, *Appl. Phys. Lett.* **2010**, *97*, 133108.
[18] N. G. Shang, P. Papakonstantinou, M. McMullan, M. Chu, A. Stamboulis, A. Potenza, S. S. Dhesi, H. Marchetto, *Adv. Funct. Mater.* **2008**, *18*, 3506.
[19] S. Campuzano, M. Pedrero, C. Montemayor, E. Fatás, J. M. Pingarrón, *J. Electroanal. Chem.* **2006**, *586*, 112.
[20] J. C. Love, L. A. Estroff, J. K. Kriebel, R. G. Nuzzo, G. M. Whitesides, *Chem. Rev.* **2005**, *105*, 1103.
[21] J. F. Masson, C. Kranz, K. S. Booksh, B. Mizaikoff, *Biosens. Bioelectron.* **2007**, *23*, 355.
[22] S. M. Richardson-Burns, J. L. Hendricks, B. Foster, L. K. Povlich, D. H. Kim, D. C. Martin, *Biomaterials* **2007**, *28*, 1539.
[23] N. Rozlosnik, *Anal. Bioanal.Chem.* **2009**, *395*, 637.
[24] E. Tamburri, S. Orlanducci, F. Toschi, M. L. Terranova, D. Passeri, *Synth. Met.* **2009**, *159*, 406.
[25] A. Kros, S. W. F. M. van Hövell, N. A. J. M. Sommerdijk, R. J. M. Nolte, *Adv. Mater.* **2001**, *13*, 1555.
[26] O. Turkarslan, S. K. Kayahan, L. Toppare, *J. Solid State Electrochem.* **2009**, *13*, 657.
[27] V. Di Noto, E. Negro, R. Gliubizzi, S. Lavina, G. Pace, S. Gross, C. Maccato, *Adv. Funct. Mater.* **2007**, *17*, 3626.
[28] Y. Zhao, L. Fan, H. Zhong, Y. Li, S. Yang, *Adv. Func. Mater.* **2007**, *17*, 1537.
[29] S. H. Joo, S. J. Choi, I. Oh, J. Kwak, Z. Liu, O. Terasaki, R. Ryoo, *Nature* **2001**, *412*, 169.
[30] L. Hutton, M. E. Newton, P. R. Unwin, J. V. Macpherson, *Anal. Chem.* **2008**, *81*, 1023.
[31] J. C. Claussen, J. B. Hengenius, M. M. Wickner, T. S. Fisher, D. M. Umulis, D. M. Porterfield, *J. Phys. Chem. C* **2011**, *115*, 20896.
[32] S. Hrapovic, E. Majid, Y. Liu, K. Male, J. H. T. Luong, *Anal. Chem.* **2006**, *78*, 5504.
[33] J. Wang, *Analyst* **2005**, *130*, 421.
[34] L. C. Clark Jr., C. Lyons, *Ann. N.Y. Acad. Sci.* **1962**, *102*, 29.
[35] J. Wang, *Electroanalysis* **2001**, *13*, 107.
[36] D. Q. Yang, E. Sacher, *Chem. Mater.* **2006**, *18*, 1811.
[37] D. Q. Yang, E. Sacher, *J. Phys. Chem. C* **2008**, *112*, 4075.
[38] C. E. Banks, T. J. Davies, G. G. Wildgoose, R. G. Compton, *Chem. Commun.* **2005**, *2005*, 829.
[39] M. Pumera, *Chem. Eur. J.* **2009**, *15*, 4970.
[40] J. F. Evans, T. Kuwana, *Anal. Chem.* **1979**, *51*, 358.
[41] S. Hrapovic, Y. Liu, K. B. Male, J. H. Luong, *Anal. Chem.* **2004**, *76*, 1083.
[42] H. Zhang, F. Jiang, R. Zhou, Y. Du, P. Yang, C. Wang, J. Xu, *Int. J. Hydrogen Energy* **2011**, *36*, 15052.
[43] S. K. M. Jonsson, J. Birgerson, X. Crispin, G. Greczynski, W. Osikowicz, A. W. Denier Van DerGon, W. R. Salaneck, M. Fahlman, *Synth. Met.* **2003**, *139*, 1.
[44] J. Lu, I. Do, L. T. Drzal, R. M. Worden, I. Lee, *ACS Nano* **2008**, *2*, 1825.
[45] S. Alwarappan, C. Liu, A. Kumar, C. Z. Li, *J. Phys. Chem. C* **2010**, *114*, 12920.
[46] S. Deng, G. Jian, J. Lei, Z. Hu, H. Ju, *Biosens. Bioelectron.* **2009**, *25*, 373.
[47] J. D. Qiu, W. M. Zhou, J. Guo, R. Wang, R. P. Liang, *Anal. Biochem.* **2009**, *385*, 264.
[48] L. Zhu, R. Yang, J. Zhai, C. Tian, *Biosens. Bioelectron.* **2007**, *23*, 528.
[49] R. B. Rakhi, K. Sethupathi, S. Ramaprabhu, *J. Phys. Chem. B* **2009**, *113*, 3190.
[50] X. Pang, D. He, S. Luo, Q. Cai, *Sens. Actuators, B* **2009**, *137*, 134.
[51] Y. Lu, M. Yang, F. Qu, G. Shen, R. Yu, *Bioelectrochemistry* **2007**, *71*, 211.
[52] X. Zeng, X. Li, L. Xing, X. Liu, S. Luo, W. Wei, B. Kong, Y. Li, *Biosens. Bioelectron.* **2009**, *24*, 2898.
[53] X. L. Luo, J. J. Xu, Y. Du, H. Y. Chen, *Anal. Biochem.* **2004**, *334*, 284.
[54] J. H. T. Luong, K. B. Male, J. D. Glennon, *Biotechnol. Adv* **2008**, *26*, 492.
[55] C. Jurysta, N. Bulur, B. Oguzhan, I. Satman, T. M. Yilmaz, W. J. Malaisse, A. Sener, *J. Biomed. Biotechnol.* **2009**, *2009*, 1.
[56] J. D. Lane, D. M. Krumholz, R. A. Sack, C. Morris, *Curr. Eye. Res.* **2006**, *31*, 895.
[57] M. Miyashita, N. Ito, S. Ikeda, T. Murayama, K. Oguma, J. Kimura, *Biosens. Bioelectron.* **2009**, *24*, 1336.
[58] L. Soleymani, Z. Fang, X. Sun, H. Yang, B. J. Taft, E. H. Sargent, S. O. Kelley, *Angew. Chem. Int. Ed.* **2009**, *48*, 8457.
[59] M. M. E. Duarte, A. S. Pilla, J. M. Sieben, C. E. Mayer, *Electrochem. Commun.* **2006**, *8*, 159.
[60] J. J. Burmeister, G. A. Gerhardt, *TrAC, Trends Anal. Chem.* **2003**, *22*, 498.
[61] P.-C. Nien, J.-Y. Wang, P.-Y. Chen, L.-C. Chen, K.-C. Ho, *Bioresour. Technol.* **2010**, *101*, 5480.
[62] A. Guiseppi-Elie, S. Brahim, G. Slaughter, K. R. Ward, *IEEE Sens. J.* **2005**, *5*, 345.
[63] K. M. Manesh, J. Halámek, M. Pita, J. Zhou, T. K. Tam, P. Santhosh, M. C. Chuang, J. R. Windmiller, D. Abidin, E. Katz, J. Wang, *Biosens. Bioelectron.* **2009**, *24*, 3569.
[64] N. G. Patel, S. Meier, K. Cammann, G. C. Chemnitius, *Sens. Actuators, B* **2001**, *75*, 101.
[65] M. Balat, H. Balat, *Appl. Energy* **2009**, *86*, 2273.